Pressure-Induced Antifluorite-to-Anticotunnite Phase Transition in Lithium Oxide

A. Lazicki[1,2], C. -S. Yoo[1], W. J. Evans[1] and W. E. Pickett[2]
[1] *Lawrence Livermore National Laboratory, Livermore, California 94550,*
[2] *Physics Department, University of California, Davis, California 95616*

Using synchrotron angle-dispersive x-ray diffraction (ADXD) and Raman spectroscopy on samples of Li_2O pressurized in a diamond anvil cell, we observed a reversible phase change from the cubic antifluorite (α, Fm3m) to orthorhombic anticotunnite (β, Pnma) phase at 50($\pm$5) GPa at ambient temperature. This transition is accompanied by a relatively large volume collapse of 5.4 ($\pm$0.8) % and large hysteresis upon pressure reversal (P_{down} at $\sim$25 GPa). Contrary to a recent study, our data suggest that the high-pressure β-phase (B_o = 188$\pm$12 GPa) is substantially stiffer than the low-pressure α-phase (B_o = 90$\pm$1 GPa). A relatively strong and pressure-dependent preferred orientation in β-Li_2O is observed. The present result is in accordance with the systematic behavior of antifluorite-to-anticotunnite phase transitions occurring in the alkali-metal sulfides.

1. INTRODUCTION

Lithium oxide (Li_2O) is one of simplest ionic oxides and it is isoelectronic to H_2O. At ambient pressure it exists in the antifluorite structure [**?**], characterized by oxygen (O^{2-}) ions arranged in an fcc sublattice with lithium (Li^{1+}) ions in tetrahedral interstitial sites (Fig. 1a). This structure is in contrast to that of isovalent symmetric ice (ice X), where the oxygen sublattice forms a bcc arrangement [**?**]. However, a further phase transformation in ice at some pressure above 150 GPa has been predicted to be antifluorite [**?** **?**]. More recent studies argue that it is either hexagonal or orthorhombic [**?**], but the nature of this phase and the pressure at which it is reached are still uncertain [**?** **?**]. In further similarity to ice, for which a high-pressure, high-temperature superionic phase has been predicted [**?**], ambient pressure Li_2O becomes superionic at temperatures above 1350 K [**?**], prior to melting at 1705 K [**?**]. In the superionic phase, oxygen ions constitute a rigid framework while lithium ions move from one tetrahedral site to another via octahedral interstitial sites. Despite its marked similarities to H_2O, until very recently the high pressure behavior of Li_2O was not addressed in the literature. One report by Kunc et al. [**?**] identified a high pressure phase transition using powder x-ray diffraction and investigated trends under pressure using *ab initio* calculations, but experimental data in this new high pressure phase is still lacking.

Technological applications for this material range from possibilities for hydrogen storage (in combination with Li_3N [**?**]), to use as a blanket breeding material for thermonuclear reactors to convert energetic neutrons to usable heat and to breed tritium necessary to sustain deuterium-tritium reactions [**?** **?**]. Understanding the behavior of Li_2O at high temperatures and pressures is therefore very useful for its applications as well as a potential aid in understanding the behavior of the hot, dense ice structures which are of such great importance to planetary science, geosciences, and fundamental chemistry. Additionally, investigation of this simple material is a reference point for understanding more complex metal-oxides.

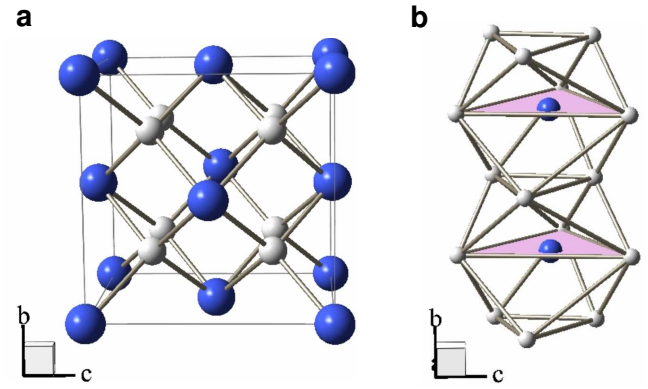

FIG. 1: (a) antifluorite α-Li_2O structure. (b) anticotunnite β-Li_2O structure showing the tri-capped trigonal prismatic coordination. Large atoms represent oxygen and smaller represent lithium.

In this study, we investigate the high pressure behavior of Li_2O at room temperature with ADXD and Raman spectroscopy. We present further and more complete evidence for a phase transition from antifluorite to anticotunnite structure, recently observed for the first time by Kunc et al. [**?**], and discuss it in light of similarities to trends observed in the alkali metal sulfides.

2. EXPERIMENT

Polycrystalline Li_2O powder (99.5% purity, CERAC, Inc.) was loaded into a membrane diamond anvil cell (DAC) of Livermore design. Brilliant cut diamonds with 0.3 mm flats were used with a 0.15 mm diameter sample chamber in a rhenium gasket of 0.05 mm initial thickness to achieve a pressure range of 8 to 61 GPa. No pressure medium was used in the experiments, although it should be noted that α-Li_2O is soft enough that non-hydrostaticity is not predicted to be a serious concern. In the first experiment copper was included in the sample chamber as an internal pressure indicator and in the

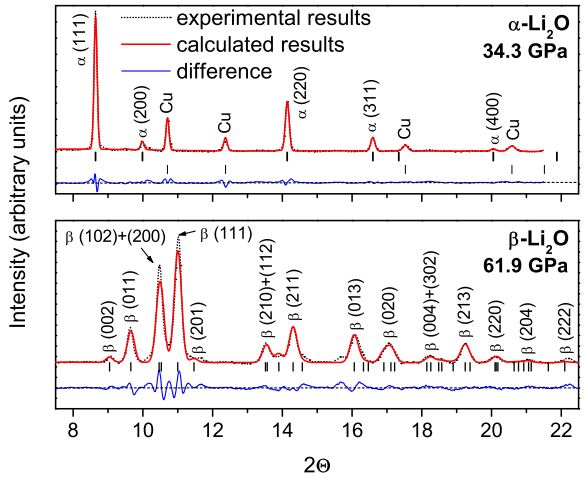

FIG. 2: Rietveld refined x-ray diffraction profile of α- and β-Li_2O. For the diffraction patterns shown, the final refinement converged to $R(F^2) = 0.1054$ for the α phase and $R(F^2) = 0.1197$ for the β phase. In the high pressure phase, only the most intense reflections are labeled. Unit cell parameters for the phase were determined from the positions of the most isolated and/or intense peaks: (002), (011), (111), (211), (013) and (020).

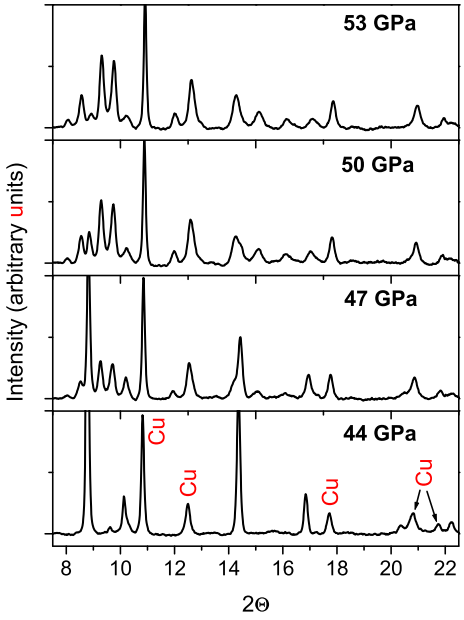

FIG. 3: Li_2O ADXD patterns across the phase transition from cubic to orthorhombic, showing the large pressure range of two-phase coexistence.

second pressure was determined from micron-sized ruby (Al_2O_3:Cr^{3+}) crystals using the quasihydrostatic ruby pressure scale [**?**]. All sample loadings were performed in an inert environment, as Li_2O is hygroscopic.

High-pressure behavior of Li_2O was investigated by ADXD and Raman spectroscopy, both at ambient temperature. ADXD was performed at the microdiffraction beamline 16IDB of the HPCAT (High Pressure Collaborative Access Team) at the APS (Advanced Photon Source). In these experiments, we used intense monochromatic x-rays ($\lambda = 0.36798$ or 0.41285 Å) microfocused to about 0.01 mm at the sample using a pair of piezo-crystal controlled bimorphic mirrors. The x-ray diffraction patterns were recorded on a high-resolution image plate detector (MAR 350). The recorded two-dimensional diffraction images (Debye-Scherrer's rings) were then integrated to produce high quality ADXD patterns using FIT2D and analyzed with the XRDA [**?**] and GSAS (EXPGUI) [**?**] programs.

Raman spectra were excited using an argon-ion laser ($\lambda = 514.5$ nm) focused to ~0.01 mm. Scattered light (measured in back-scattering geometry) was filtered with a 514.5 nm Super-Notch-Plus filter, analyzed with a single spectrometer (characterized by less than 3 cm^{-1} spectral resolution) consisting of a 1200 grooves/mm ion-etched blazed holographic diffraction grating, and imaged with a liquid nitrogen cooled CCD camera at Lawrence Livermore National Laboratory. A spectral range of 10-1400 cm^{-1} was used.

3. X-RAY DIFFRACTION

Rietveld refinements of the ADXD patterns of Li_2O confirm the identity of the antifluorite (α-Li_2O) structure (Fig. 2, top panel), which is found to be stable up to 45 GPa. Above this pressure, diffraction peaks from a new phase begin to emerge, as shown in Fig. 3. However, traces of the low-pressure phase are apparent up to nearly 55 GPa. This large coexistence region may be due to pressure gradients in the cell which arise because of a lack of pressure medium. This seems unlikely, however, because all diffraction peaks remain relatively sharp across the transition and also Kunc et. al. [**?**] demonstrate that, at the onset of the phase transition, the shear stress conditions become more uniform. In a homogeneous sample, such a coexistence region may be due to hysteresis arising from nucleation barriers to a first-order transition, or it may indicate that this transition is kinetically hindered or sluggish. These explana-

TABLE I: lattice parameters and fractional coordinates for β-Li_2O at 61.5 GPa

Lattice parameters	**a(Å)**	**b(Å)**	**c(Å)**
(61.5 GPa)	4.45(6)	2.786(4)	5.21(2)
Fractional coordinates	**x**	**y**	**z**
O	0.745	0.25	0.600
Li(1)	0.883	0.25	0.305
Li(2)	0.305	0.25	0.570

tions seems much more likely, and are consistent with an even larger (25 GPa) hysteresis that was observed upon pressure reversal, as will be shown.

The Cu pattern in the x-ray diffraction diagrams of Fig. 3 is undesirable for a clean refinement of crystal structure, particularly so for the high-pressure phase where several reflections from Cu overlap with those from the sample. We performed an additional experiment without Cu (but with ruby) and carried out a full Rietveld profile refinement of the structure based on the anticotunnite (β-Li_2O) structure ($PbCl_2$-type, Pnma, Z = 4) identified in [**?**], and also seen in the similar alkali metal sulfide Li_2S system [**?**]. Clearly, the refined results (summarized in Fig. 2, lower panel) are reasonably good even at 61.9 GPa. The starting atomic coordinates were those determined for Li_2S in the Pnma structure at 7.9 GPa; a = 5.92 Å, b = 3.65 Å, c = 6.90 Å, $x_O = 0.77$, $x_{Li1} = 0.98$, $x_{Li2} = 0.32$, $z_O = 0.61$, $z_{Li1} = 0.36$, $z_{Li2} = 0.56$. Refined parameters include cell parameters, profile function, fractional coordinates, thermal parameters, Chebyshev polynomial background and the spherical harmonic (6^{th} order) correction for preferred orientation (PO). The final refinement converges to $R(F^2) = 0.1197$, with atom positions given in Table 1. At this pressure, a refinement of the PO correction yielded a texture index of 1.5437, indicating a moderate PO in the orthorhombic phase at 61.9 GPa. This effect is confirmed by the presence of clear intensity variations around the powder diffraction rings shown in Fig. 4. Because of the quality of our data the refinement was not entirely conclusive, and the resulting structure must, therefore, be viewed as approximate.

The crystal structure of β-Li_2O can be understood to consist of chains of distorted tricapped trigonal prisms of cations parallel to the y-axis, giving the anion a coordination number of 9 (Fig. 1b). Near the transition, the polyhedral cation-anion distances range from 1.664 Å to 2.246 Å with an average of 1.89 Å. These values are reasonable, based on the Li-O distances quoted for lithium oxide clusters in [**?**]. In comparison, in the α-Li_2O structure, the anion coordination number is 8 with a cation-anion distance of 1.79 Å near the transition. There is a 5.4 ± 0.3 % volume collapse across the transition.

Between 53 and 61 GPa (these two diffraction patterns were taken during separate experiments), we observe an inversion in relative intensities of the two most prominent peaks. The first is a superposition of the (102) and more intense (200) reflections and second is the (111) reflection. At 53 GPa, the presence of copper in the diffraction pattern and also the remnant peaks from the cubic phase make an accurately detailed analysis impracticable. But we observe that it is possible to effect such an intensity inversion by lowering the PO correction from the value found to be necessary at 61.9 GPa. It is therefore likely that the changes in peak intensities are due to the expected increase in PO with pressure, evident from Fig. 4. In the study of Li_2S by Grzechnik et al. [**?**], the observation of an inversion of relative intensities of the (011) and (111) peaks led them to successfully employ a two-phase refinement based on a mixture of the anticotunnite phase and another phase with the $Pn2_1a$ space group, which allows for more freedom in the lithium positions. An attempt to apply a similar model to Li_2O failed at lower pressures because of inadequate signal quality, and at 61.9 GPa it did not result in any marked improvement of the refinement. In order to understand what, if any, distorted intermediate phases may arise between the α and β structures, more detailed diffraction patterns must be acquired, particularly at higher 2Θ, between 50 and 60 GPa.

Fig. 5 shows the pressure-volume data of the two phases, along with the best fit 3^{rd} order Birch-Murnaghan equation of state (EOS) curves. Also shown are experimental data points and calculated EOS curves from [**?**]. Fitting parameters are summarized in Table II. Because of a limited pressure range studied for β-Li_2O, it was necessary to constrain B' to equal 4. This approximation was based on the procedure adopted by Grzechnik et al. [**?**] in the case of Li_2S. Variation of this value between 3.5 and 4.5 resulted in at most a 12% difference in B_o and a 1% difference in V_o. There is a dramatic disparity between the equations of state for the orthorhombic phase found in the present study and the previous one[**?**]. The β-Li_2O pressure-volume data from [**?**], however, are not taken from experiment but generated from *ab initio* total energy DFT calculations, using the Projector Augmented Waves (PAW) method. In the high pressure phase, they determined the lattice parameters and internal positions by a process of 'relaxing' these

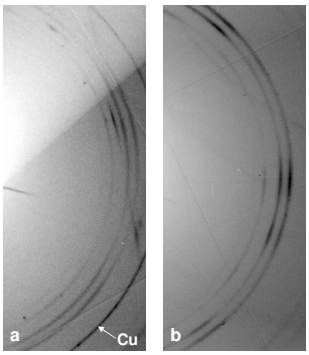

FIG. 4: Powder diffraction rings of γ-Li_2O at 53 GPa (a) and 61 GPa (b), showing the presence of texture in this phase, and the increase in preferred orientation with pressure. The three most prominent rings shown are the (011), (102)+(200), and (111) reflections.

TABLE II: Birch-Murnaghan EOS fitting parameters. Volumes are given per formula unit.

	B_o (GPa)		V_o (Å^3)		B'	
	This work	[**?**]	This work	[**?**]	This work	[**?**]
α	90(1)	75(7)^a	24.24(2)	24.69(9)^a	3.51(5)	5.2(7)^a
β	188(12)	80.8(18)^b	20.0(2)	23.51(6)^b	4 (fixed)	3.92(6)^b

^{a}Experimental results
^{b}Calculated results

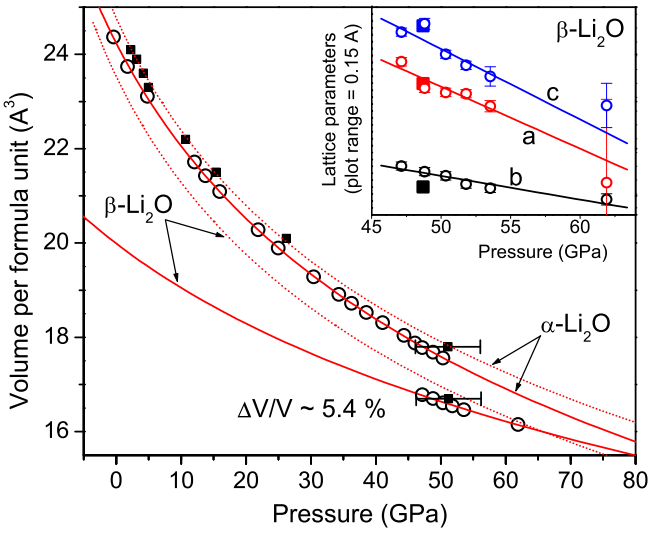

FIG. 5: EOS for the two Li_2O phases. In the main plot, solid curves are the Birch-Murnaghan EOS fits to the experimental data (shown as open circles) in this study. Solid squares are the experimental data from [**?**] and dotted curves are the theoretically calculated EOS [**?**] for both phases. Inset: trends in the evolution with pressure of the lattice parameters in the β phase. Empty circles are data from this study (error bars shown when they exceed size of data points), and solid squares are experimental data from [**?**].

parameters, minimizing all forces at each step. In the experiment, however, the proposed rapid increase in PO with pressure may also suggests a rapid increase in stress inhomogeneity as well, a state which is not well modeled by the 'relaxed' structure in the calculation. The use of an optimally hydrostatic pressure medium in a future experiment may indicate just how well the theoretical model approximates reality in this case.

The dramatic factor-of-two increase in bulk modulus across this phase transition appears anomalously large, but actually a similar (and larger, at 160%) increase is recorded for the antifluorite-anticotunnite transition in Li_2S [**?**] and, although values for bulk modulus are not quoted, it appears that a similar effect is seen in Na_2S [**?**]. Also, in spite of the differences between the equations of state given here and in [**?**], it should be noted that the one experimental data point shown for the high pressure phase in [**?**] (reproduced in Fig. 5), does agree quite well with the present work. An examination of the pressure evolution of the a, b and c lattice parameters, shown in the inset of Fig. 5, goes further to explain the large increase in bulk modulus. We find that the b-axis is much stiffer (almost three times greater) than the a and c axes. Thus, the trigonal prism chains shown in Fig. 1b are seen to be very rigid and to strongly resist compression. This is consistent with the sizable directional effects which are apparent from the increase in preferred orientation.

4. RAMAN SPECTROSCOPY

The pressure-induced changes in Raman spectra of Li_2O give further evidence of a phase transition beginning near 49 GPa upon increasing pressure as shown in Figure 6. The low-pressure α phase has four formula units per unit cube. Factor group analysis gives one Raman active optical phonon mode T_{2g}, which describes motion of the Li sublattice. This mode is seen in the Raman spectrum near 575 cm^{-1} at low pressure. At the phase transition from α to β there is a considerable lowering of symmetry and consequently a significant increase in number of modes. The β phase has four formula units per unit cube, and factor group analysis yields $6A_g + 3B_{1g} + 6B_{2g} + 3B_{3g}$ Raman active phonon modes. In the Raman spectrum of the β phase, we see three prominent bands (near 750, 800 and 830 cm^{-1}) and at least seven weaker bands at lower Raman shifts, not counting even weaker features appearing as shoulders of these bands. Since the sample is powder, a precise mode assignment for the Raman peaks is difficult. The observation of fewer modes than predicted by group theory is likely due to accidental degeneracy, insufficient instrumental resolution, and/or diminishingly weak intensity.

The pressure-induced shifts of the distinguishable Raman bands are plotted in Figure 7, observed in both up (solid circles) and down (open circles) strokes of pressure. Experimental data and theory curves from [**?**] are also shown, for comparison. Data points are fit with an equation of state derived from valence force field theory which was previously shown to be physically realistic [**?**]. The frequency shifts with pressure, represented as:

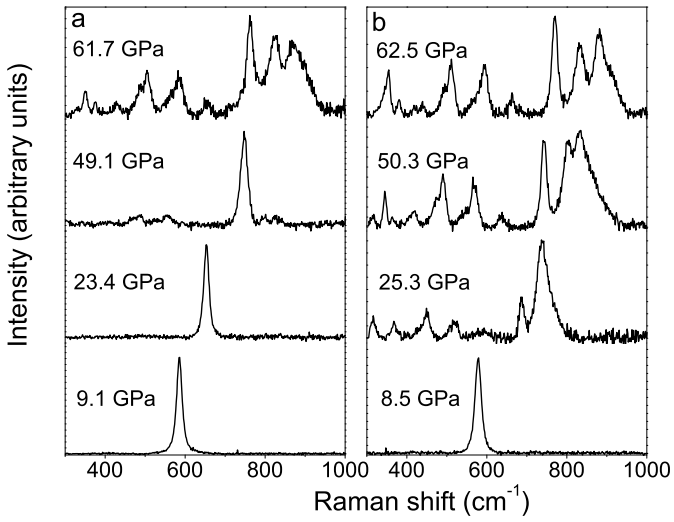

FIG. 6: Raman spectra upon increasing (a) and decreasing (b) pressure. Cosmic radiation spikes were removed from two of the spectra.

$$\left(\frac{\partial\omega}{\partial P}\right)_{P=50\ GPa} \quad (1)$$

are printed in Fig. 7 for each Raman band. The Raman band in the α phase shifts much more rapidly than those in the β phase - a further confirmation of a large difference in bulk modulus. The dotted lines represent the approximate transition pressures upon increasing and decreasing pressure. There is a large (nearly 25 GPa) hysteresis in this transition (also seen in panel b of Fig. 6) and when decreasing pressure the $\beta \rightarrow \alpha$ transition occurs near 25 GPa. Several of the orthorhombic Raman bands can be seen to overlap and undergo changes in relative intensity in the pressure region that is inaccessible when increasing pressure. Kunc et al. [**?**] observed a similar hysteresis and the data from their Raman experiment agrees well with the present study. Their calculated results (shown as dotted curves) for the α phase are also in very good agreement; the curve is almost perfectly aligned with our experimental data in that phase. The β phase calculated phonon mode shifts, however, show a marked disagreement. Nevertheless, this is not surprising as their EOS describes a much softer material with much more homogeneous stress conditions, so the Raman bands would be expected to occur at a lower frequency, and would shift more rapidly with pressure, as indeed the calculations predict.

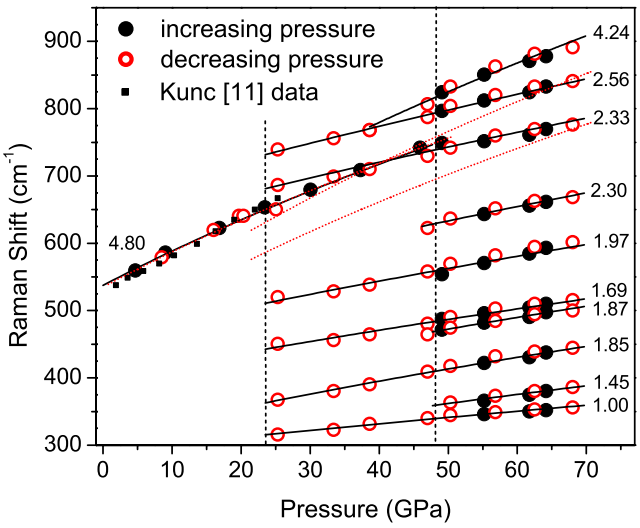

FIG. 7: The shift in pressure of Li_2O Raman bands. Individual Raman bands are labeled with the pressure derivative of the Raman frequency at 50 GPa. Solid lines are fits to the experimental data from this study. Red dotted lines represent the calculated theoretical pressure dependence of the Raman frequencies from [**?**]. In the cubic phase, the theoretical curve lines up exactly with the experimental result from this study. Vertical dashed lines approximate the phase transition pressure upon increasing and decreasing pressure.

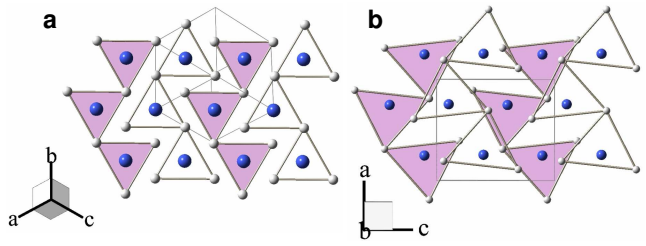

FIG. 8: (a) α-Li_2O along the (111) plane, showing the transition mechanism to β-Li_2O (b). For the cubic structure shown in (a), all oxygen ions are all coplanar, located midway between planes of lithium ions which are separated by 1.032 Å near 50 GPa. For the orthorhombic structure shown in (b), half the oxygen ions have moved into the lower plane of Li ions (shown as colored polyhedra) and half into the upper (empty), with the planes separated by 1.402 Å near 50 GPa.

5. DISCUSSION

The mechanism for the antifluorite-anticotunnite phase transition is already well understood because of the numerous well-known pressure-induced fluorite-cotunnite transitions that occur [**?** **?**]. If one pictures the antifluorite structure as (111) planes of anions separated by pairs of (111) planes composed of ions from the cation sublattice, the mechanism for the transition to anticotunnite can be seen as a displacement of the anions in the [111] directions, half to the adjacent upper plane and half to the adjacent lower plane, accompanied by slight rotations and distortions of the Li triangular polyhedra within the planes. (Fig. 8.) This transition has the advantage of increasing the oxygen coordination number from 8 to a more stable 9, increasing the average oxygen-lithium separation distance from 1.78 Å to 1.89 Å, and increasing the packing through the 5.4 % volume collapse from 17.56 Å^3/formula unit to 16.61 Å^3/formula unit near 50 GPa. At this pressure, the α-Li_2O phase lattice parameter is a = 4.126 Å while the β-Li_2O phase parameters are given by a = 4.518 Å, b = 2.808 Å, c = 5.246 Å. Accompanying this transition is a remarkable 100 GPa increase in bulk modulus, for which an inhomogeneous stiffening of the material along the b-axis is at least partially responsible. The repulsion between closely spaced and highly charged ions contributes to the overall stiffening of the crystal lattice. At pressures this high, the distance between highly charged ions is small enough that, in order to overcome the columbic repulsions which threaten to destabilize the structure, the coordination number needs to be high around the most highly charged (O^{2-}) ions. Therefore, a transition to an Ni_2In-type structure is expected at even higher pressure, as it would further increase the anion coordination number to 11.

An examination of the known behavior of alkali-metal chalcogenides under pressure may allow us to understand and predict the behavior of this class of materials. Al-

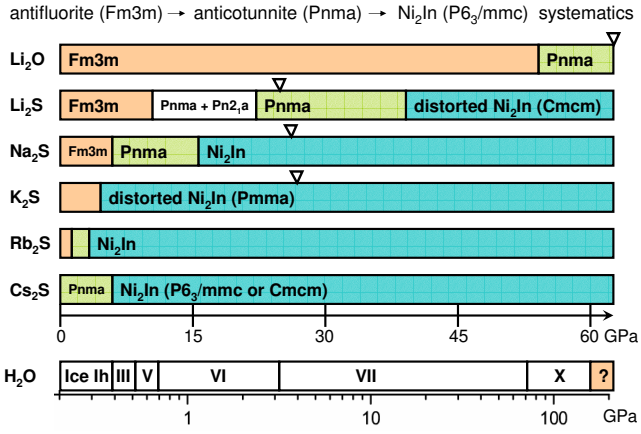

FIG. 9: Comparison of Li_2O pressure behavior with that of the alkali-metal sulfides. H_2O may transition to a cubic antifluorite-type phase above 170 GPa, and, in the nonmolecular form, may be expected to follow the same trends as the alkali metal chalcogenides. $\bigtriangledown$ represents the high pressure limit of experiments.

though Li_2O is the first alkali-metal oxide which has been shown to possess a pressure-induced antifluorite-anticotunnite transition, it is relatively common in alkali-metal sulfides. [**?** **?** **?**] Li_2S, Na_2S, K_2S, and Rb_2S have all been shown or are predicted to undergo an antifluorite to anticotunnite transition, at lower and lower pressures with increasing cation mass until, in Cs_2S, the anticotunnite phase is stable at ambient conditions (Fig. 9). These compounds are predicted to undergo a second transition from the anticotunnite to a hexagonal Ni_2In-type phase at even higher pressure [**?**] and so it is likely that Li_2O will do the same, although the calculations of Kunc et al., [**?**] indicate that this will not occur below 100 GPa.

Alkali metal oxides K_2O, Na_2O and Rb_2O also have the antifluorite structure at ambient conditions [**?** **?**]. The only alkali metal oxide exception is Cs_2O, which has been seen to possess the $CdCl_2$ structure [**?**] which, however, is a simple rhombohedral distortion of the fluorite structure. No high-pressure studies have been performed on these materials, but we can reasonably expect that they will follow the same series of transitions that have been observed here. Ice also, in the past, has been predicted to exist in the antifluorite structure at sufficiently high pressure [**?** **?**]. Since then this proposition has been called into question, but the actual high pressure structure remains to be seen experimentally, and is most currently not predicted to exist below 170 GPa [**?**]. Ice VII gradually becomes "symmetric" ice-X at the pressure range of 40-90 GPa, with a bcc oxygen sublattice, similar to that of ice VII but with hydrogen atoms occupying the central position between adjacent oxygen atoms. The possibility of a transition of ice X to a phase similar to that of α-Li_2O could indicate a systematic pressure-induced structural behavior for all alkali-metal chalcogenides.

6. CONCLUSION

A recently discovered pressure-induced antifluorite-anticotunnite phase transition, seen for the first time in an alkali-metal chalcogenide [**?**], was investigated in detail using x-ray diffraction and x-ray Raman scattering. Several new properties of the high pressure phase were discovered. A dramatic increase in bulk modulus was seen for the first time, and the source of the high pressure phase's rigidity identified to be related to an inhomogeneous stiffening of one of the crystal lattice parameters. A consequent large increase in preferred orientation in the orthorhombic phase was also identified during the Rietveld refinement as responsible for an inversion in the intensities of two of the most prominent x-ray diffraction peaks. The pressure-induced shift in the Raman bands of both phases were observed, and found to be consistent with our observation of a large bulk modulus increase. The x-ray diffraction and Raman data both point towards a strong hysteresis across this transition, which is consistent with a kinetically hindered or sluggish first-order transition, or one in which a large volume change and a large change in bulk modulus can serve as nucleation barriers for the transition. Comparisons were drawn between Li_2O and a series of alkali metal sulfides, allowing us to make confident predictions about the high pressure behavior of the rest of the alkali-metal chalcogenides and even, perhaps, the behavior of dense, nonmolecular ice at ultrahigh pressures.

ACKNOWLEDGMENTS

We would like to thank J. P. Klepeis for many helpful discussions. This work has been supported by the LLNL, University of California, under the auspices of the U.S. DOE under Contract No. W-7405-ENG-48 and by the Stockpile Stewardship Academic Alliances Program under grant DOE 01-06NA26204. Use of the HPCAT facility was supported by DOE-BES, DOE-NNSA (CDAC, LLNL, UNLV), NSF, DOD-TACOM, and the W. M. Keck Foundation. We thank HPCAT beamline scientist Maddury Somayazulu for technical assistance.

[] F. A. Shunk (Ed.), Constitution of Binary Alloys, 2nd Suppl. (McGraw-Hill, New York, 1969).
[] K. R. Hirsh and W. B. Holzapfel, Phys. Lett. **101A**, 142 (1984).
[] P. Demontis, R. LeSar and M. L. Klein, Phys. Rev. Lett. **60**, 2284 (1988).

[] P. Demontis, M. L. Klein and R. LeSar, Phys. Rev. B **40**, 2716 (1989).
[] M. Benoit, M. Bernasconi, P. Focher and M. Parrinello, Phys. Rev. Lett. **76**, 2934 (1996).
[] P. Loubeyre, R. LeToullec, E. Wolanin, M. Hanfland and D. Hausermann, Nature **397**, 503 (1999).
[] M. Benoit, A. H. Romero and D. Marx, Phys. Rev. Lett. **89**, 145501-1 (2002).
[] C. Cavazzoni, G. L. Chiarotti, S. Scandolo, E. Tosatti, M. Bernasconi and M. Parrinello, Science **283**, 44 (1999).
[] S. Hull, T. W. D. Farley, W. Hayes and M. T. Hutchings, J. Nucl. Mater. **160**, 125 (1988).
[] Y. Y. Liu, M. C. Billone, A. K. Fischer, S. W. Tam and R. G. Clemmer, J. Fusion Technol. **8**, 1970 (1985).
[] K. Kunc, I. Loa, A. Grzechnik and K. Syassen, Phys. Status Solidi B **242**, 1857 (2005).
[] Y. H. Hu and E. Ruckenstein, Ind. Eng. Chem. Res. **43**, 2464 (2004).
[] S. Tanaka, M. Taniguchi and H. Tanigawa, J. Nucl. Mater. **283-287**, 1405 (2000).
[] K. Noda, K. Uchida, T. Tanifuji and S. Nasu, Phys. Rev. B **24**, 3736 (1981).
[] H. K. Mao, J. Xu and P. M. Bell, J. Geophys. Res. **91**, 4673 (1986).
[] S. Desgreniers and K. Lagarec, J. Appl. Cryst. **31**, 109 (1998).
[] B. H. Toby, J. Appl. Cryst. **34**, 210 (2001).
[] A. Grzechnik, A. Vegas, K. Syassen, I. Loa, M. Hanfland and M. Jansen, J. Solid State Chem. **154**, 603 (2000).
[] F. Finocchi and C. Noguera, Phys. Rev. B **53**, 4989 (1996).
[] A. Vegas, A. Grzechnik, K. Syassen, I. Loa, M Hanfland and M. Jansen, Acta Crystallogr., Sect. B: Struct. Sci. **57**, 151 (2001).
[] W. A. Van Uden, H. Hubel, J. M. Hayes, A. D. Prins, M. Kuball, D. J. Dunstan, J. R. Downes, Y. Ying Shi and J. H. Edgar, High Press. Res. **22**, 27 (2002).
[] L. Gerwald, J. S. Olsen, S. Steenstrup, M. Malinowski, S. Åsbrink and A. Waskowska, J. Appl. Crystallogr. **25**, 578 (1992).
[] J. M. Leger, J. Haines, A. Atouf, O. Schulte and S. Hull, Phys. Rev. B **52**, 13247 (1995).
[] J. C. Schön, Ž. Čančareić and M. Jansen, J. Chem. Phys. **212**, 2289 (2004).
[] R. Dovesi, C. Roetti, C. Freyria-Fava, M. Prencipe and V. R. Saunders, Chem. Phys. **156**, 11 (1991).
[] CRC Handbook of Chemistry and Physics, David R. Lide, (Ed.), 79th Edition (CRC Press, Boca Raton, FL 1998).
[] K. R. Tsai, P. M. Harris and E. N. Lassettre, J. Phys. Chem. **60**, 338 (1956).